

TOPOLOGICAL TRAPS IN EVOLUTIONARY GAMES

JOSE SEGOVIA-MARTIN¹

ABSTRACT. How cooperation originates and persists among self-interested individuals is a central question in the social and behavioural sciences. In the canonical two-dimensional spatial Prisoner’s Dilemma with unconditional imitation introduced by Nowak and May (1992), simulations on a Moore lattice show an abrupt drop in cooperation near the temptation $T \approx 5/3$, yet even under these harsh conditions cooperative structures can still arise. However, the nucleation rates of these motifs, and their contribution along the full cooperation curve had not been quantified. Here we show, using large-scale Monte Carlo simulations combined with automatic cluster classification, that on the Moore lattice for $T \geq 5/3$ residual cooperation is sustained exclusively by 3×3 (or larger) rectangular cooperator bricks, whereas on degree-8 random-regular graphs for $T \gtrsim 1.5$ it is dominated by star-like motifs (1 hub + 8 leaves). Once the dynamics becomes nucleation limited, the macroscopic cooperation level is therefore governed by the statistics of a few exceptionally resilient shapes, rather than by many different cooperator motifs. Furthermore, we show that the lattice cooperation collapse near $T = 5/3$ is kinetic rather than critical: the reduction in cooperation is not due to a loss of growth capacity of rectangular bricks, but to the progressive destabilisation of the subcritical motifs that dominate just below this threshold. Our results show that residual cooperation at high temptation is a rare-event nucleation phenomenon governed by a small set of topological traps, and highlight the value of motif-level analysis for explaining and engineering cooperation in spatial, social, and technological networks.

1. MAIN

The persistence of cooperation among unrelated, self-interested agents is a long-standing puzzle that permeates the natural and social sciences [1, 2, 3]. Formally, the puzzle is epitomised by the Prisoner’s Dilemma (PD): although mutual cooperation delivers the highest collective welfare, unilateral defection strictly dominates and is the only Nash equilibrium in a well-mixed population [4, 5, 6]. Among the many mechanisms proposed to overcome this dilemma (direct reciprocity, kin selection, punishment, reputation, *inter alia*), *network reciprocity* (the idea that the pattern of who interacts with whom matters) remains one of the most influential and best quantified [7, 8, 9].

The *Prisoner’s Dilemma* (PD) is the archetypal 2×2 game that formalises the conflict between individual and collective interests. Each player chooses either to *cooperate* (C) or *defect* (D). If both cooperate they each receive the *reward* payoff R ; if both defect they receive the lower *punishment* payoff P . When one defects while the other cooperates, the defector earns the highest *temptation* payoff T and the cooperator suffers the lowest *sucker’s* payoff S . The ordering

$$T > R > P > S$$

ensures that defection strictly dominates cooperation: irrespective of the opponent’s move, D yields a higher individual payoff than C . Consequently the unique Nash equilibrium is mutual defection (D, D) , even though mutual cooperation (C, C) maximises the collective return $2R$. The PD thus encapsulates the core paradox of cooperation and motivates the search for mechanisms (reciprocity, kin selection, punishment, network structure, *etc.*) capable of sustaining cooperative behaviour.

Evolutionary game theory provides the mathematical language in which these mechanisms are typically explored. In well-mixed (mean-field) settings the standard description is the *replicator equation*, first derived by Taylor and Jonker and later reviewed in depth by Hofbauer and Sigmund [10, 11]. The replicator dynamics link the growth rate of each strategy to its excess payoff over the population average and retain the classical Nash-equilibrium concept [12] as their fixed points. On graphs, however, individuals update their strategies through local rules that need not mirror the replicator flow. Among the most studied is *unconditional imitation* (UI): after each round every player adopts the strategy of the neighbour with the highest payoff, provided that payoff is strictly larger than her own [7]. Despite its extreme simplicity, UI captures an important behavioural heuristic (i.e., “copy success”) and, crucially, breaks the symmetry between cooperators and defectors in spatial

Key words and phrases. Game Theory | Complex Networks | Cooperation.

PD [8, 9]. When embedded in a regular lattice this rule creates positive feedback, where a lone cooperator can recruit neighbouring defectors, enlarge a compact cluster, and thereby raise its own payoff even further. The collective outcome is a cooperation plateau that cannot be anticipated from simple mean-field analysis and that depends sensitively on both the network structure and the details of the update process.

The seminal lattice study by Nowak and May showed that, under *unconditional imitation*, spatial clustering of cooperators can protect them from invasion and generate a striking “staircase” dependence of the asymptotic cooperator fraction on the temptation to defect T [7]. In plain terms, their simulations revealed that once a few neighbours begin cooperating they can form a compact “island” that shields its members from being overtaken by defectors. As long as the temptation T is not too large, these cooperative islands survive and even spread, but above certain T thresholds they are finally eroded away. Subsequent work has generalised those findings to a broad spectrum of update rules, graph topologies and evolutionary time scales [13, 14, 15]. Yet, more than three decades after the seminal study of Nowak and May, several questions remain open:

- Q1:** *Which concrete cooperator motifs sustain the successive cooperation plateaux on different graphs?*
- Q2:** *Does the abrupt drop in cooperation at intermediate temptation T correspond to a true phase transition, or is it a kinetic bottleneck caused by the extinction of specific motifs?*
- Q3:** *Which motifs account for the residual cooperation observed beyond the critical value of T ?*

Analytical treatments of the spatial Prisoner’s Dilemma on Nowak and May 2D lattices demonstrate that compact blocks of cooperators forming a rectangular $k \times l$ cluster with $k, l \geq 3$ cannot be invaded even for $5/3 < T < 8/3$ when $(R, S, T, P) = (1, 0, T, 0)$ [8]. These facts suggest that compact bricks could be natural candidates to sustain the lattice cooperation plateau, yet their actual nucleation rate and role in the full cooperation curve have not been quantified. Determining how the availability of these motifs changes across T is therefore one of the central aims of the present study.

Random-regular (RR) networks with the same degree k offer a natural counterpoint to the lattice benchmark because they are locally tree-like. In random regular graphs the concentration of short loops vanishes as $N \rightarrow \infty$, so local neighbourhoods become increasingly similar to a tree [8]. Using RR graphs therefore lets us hold fixed the key ingredients of the Nowak and May setting (network size, degree, payoff structure, and update rule) while removing the geometric embedding that supports compact blocks on lattices. We therefore study the same PD dynamics on RR graphs and quantify (i) which cooperator motifs appear, (ii) how often they nucleate as the temptation T varies, and (iii) how their growth or extinction shapes the macroscopic cooperation curve. A key focus is the high temptation regime. We identify the specific clusters that survive at the largest T and test whether residual cooperation there is explained by the rare nucleation of a small set of exceptionally resilient motifs.

By comparing the motif census on the lattice and on RR graphs we isolate which structural features govern motif availability, completion, and long-run persistence, thereby linking microscopic cluster dynamics to macroscopic cooperation across topologies.

2. METHODS

This section specifies the model and simulation protocol. Section 2.1 describes the network structure, namely either a 100×100 Moore degree-8 lattice (following Nowak and May [7]) or a degree-8 random-regular (RR) graph on $N = 10^4$ nodes. Section 2.2 details the strategy initialisation, where each node starts as a cooperator or defector with equal probability, the payoff structure, namely a standard Prisoner’s Dilemma matrix with $R = 1$, $S = P = 0$ and temptation $T \in [1, 2]$, and the deterministic unconditional imitation update rule, whereby at every synchronous time step each player compares its payoff with those of its neighbours and adopts the strategy of the highest-payoff neighbour whenever that payoff is strictly higher than its own. We scan over T , simulate each configuration for 100 time steps, and for every pair (network type, T) average over 1000 independent repetitions differing only in their random initial conditions. Section 2.3 describes the recorded observables: (i) the global cooperation level and the proportions of “consistent- C ,” “consistent- D ,” and “oscillator” nodes (based on the last two strategies), and (ii) the connected components of the cooperator subgraph, which are automatically labelled rectangle, star, chain, loop, compact, cycle, irregular, etc. using simple geometric and graph-theoretic descriptors (bounding-box dimensions, fill ratio, perimeter, interior holes, approximate diameter), together with their temporal classification into stable and unstable clusters.

2.1. Network structure. We consider two network topologies with the same number of nodes and degree. 2D lattice. The first topology is a two-dimensional spatial lattice with periodic boundary conditions, forming a Moore neighbourhood for each node. This network consists of $N = 10,000$ nodes arranged in a 100×100 grid, where each node is connected to its eight nearest neighbours (four von Neumann neighbours plus four diagonals). The periodic boundary conditions make the lattice topologically equivalent to a torus, avoiding edge effects.

Random-regular network. For comparison we consider a homogeneous random network with the same size and degree. Let $\mathcal{G}_{N,k}$ denote the ensemble of all simple, undirected k -regular graphs on N labelled vertices. For $N = 10^4$ and $k = 8$ we draw a single graph $G = (V, E) \sim \text{Uniform}(\mathcal{G}_{N,8})$, so that every node $i \in V$ has exactly $|\mathcal{N}(i)| = 8$ neighbors, but without any lattice structure. This random-regular graph is kept fixed while we vary the game parameter T and run multiple stochastic realisations of the dynamics.

In both topologies the interaction graph is thus simple, undirected and 8-regular on $N = 10^4$ vertices.

2.2. Strategies and Initialisation. Each node i in the network adopts a binary strategy, $s_i \in \{0, 1\}$, where 0 represents defection and 1 represents cooperation. At the start of each simulation, strategies are assigned randomly, with each node having an equal probability of adopting either strategy:

$$P(s_i = 0) = P(s_i = 1) = 0.5.$$

2.2.1. Payoff Structure. The interactions between nodes are governed by the standard Prisoner's Dilemma payoff matrix:

	<i>C</i>	<i>D</i>
<i>C</i>	(<i>R, R</i>)	(<i>S, T</i>)
<i>D</i>	(<i>T, S</i>)	(<i>P, P</i>)

where $R = 1$ (reward), $S = 0$ (sucker's payoff), $P = 0$ (punishment), and T (temptation) is varied in the interval $[1, 2]$. In practice we explore T on the discrete grid

$$T \in \{1.00, 1.05, \dots, 2.00\} \cup \{1.66, 1.67, 1.68\}.$$

The total payoff Π_i of node i is determined by summing the payoffs from pairwise interactions with its neighbours:

$$\Pi_i = \sum_{j \in \mathcal{N}_i} \pi(s_i, s_j),$$

where \mathcal{N}_i is the set of neighbours of node i , and $\pi(s_i, s_j)$ denotes the payoff obtained by i when interacting with neighbour j . The payoffs for all possible strategy combinations are:

$$\pi(1, 1) = R, \quad \pi(1, 0) = S, \quad \pi(0, 1) = T, \quad \pi(0, 0) = P.$$

2.2.2. Update Rule: Unconditional Imitation. The strategy update follows the unconditional imitation rule. At each time step t , each node i evaluates the total payoffs of itself and its neighbours:

$$\Pi_j(t), \quad \forall j \in \mathcal{N}_i \cup \{i\}.$$

Node i adopts the strategy of the neighbour (or itself) with the highest payoff:

$$j^* = \arg \max_{j \in \mathcal{N}_i \cup \{i\}} \Pi_j(t), \quad s_i(t+1) = \begin{cases} s_{j^*}(t), & \Pi_{j^*}(t) > \Pi_i(t), \\ s_i(t), & \text{otherwise.} \end{cases}$$

If the highest payoff is not strictly greater than its own, the node keeps its strategy.

2.2.3. Computational Implementation. The simulations were implemented in Python using the NetworkX library to construct both the lattice and random-regular networks and to manage neighbour relationships. Parallel computation was employed using the multiprocessing library. For each value of T and each network type, the 1000 independent runs were distributed across available CPU cores.

2.3. Recorded quantities and cluster analysis. To characterise the emergent patterns of cooperation, at each time step t and for each simulation run we record both global and meso-scale descriptors.

2.3.1. *Global cooperation level.* Let $s_i(t) \in \{0, 1\}$ denote the strategy of node i at time t , with $1 \equiv C$ (cooperate) and $0 \equiv D$ (defect). The global fraction of cooperators is

$$f_C(t) = \frac{1}{N} \sum_{i=1}^N s_i(t).$$

2.3.2. *Strategy dynamics classification.* For each node i and each time $t \geq 1$ we maintain a rolling history of the two most recent strategies $(s_i(t-1), s_i(t))$. On this basis we classify nodes into three types:

Consistent cooperators: $s_i(t-1) = s_i(t) = 1$;

Consistent defectors: $s_i(t-1) = s_i(t) = 0$;

Oscillators: $s_i(t-1) \neq s_i(t)$.

At each time step we record the proportion of nodes in each category, which summarises the stability and volatility of individual strategies.

2.3.3. *Cooperator subgraph and connected components.* Let $G = (V, E)$ denote either the lattice or the random-regular graph. The cooperator subgraph at time t is defined as

$$G_C(t) = (V_C(t), E_C(t)), \quad V_C(t) = \{i \in V : s_i(t) = 1\}, \quad E_C(t) = \{\{u, v\} \in E : u, v \in V_C(t)\},$$

where $V_C(t)$ is the set of cooperating nodes, and $E_C(t)$ the set of edges whose endpoints are both cooperators.

We decompose $G_C(t)$ into its connected components,

$$\mathcal{K}(t) = \{K^{(\ell)}(t) : \ell = 1, \dots, m_t\},$$

so that $\mathcal{K}(t)$ is the set of all connected components of $G_C(t)$. For each component $K \in \mathcal{K}(t)$ we denote

$$n_K = |K|, \quad e_K = |\{\{u, v\} \in E_C(t) : u, v \in K\}|,$$

where n_K is the number of nodes in K and e_K the number of edges with both endpoints in K .

We extract the following geometric and topological descriptors:

Perimeter nodes (lattice only). On the Moore lattice we view clusters on the underlying $\sqrt{N} \times \sqrt{N}$ grid and use the von Neumann (4-neighbour) structure to define their boundary. For a cooperator component $K \subset V_C(t)$, let

$$P_K = |\{v \in K : \text{fewer than four of its von Neumann neighbours belong to } K\}|$$

be the number of boundary cooperators in K .

Compactness (lattice only).

$$\kappa_K = \frac{n_K}{P_K} \quad (\text{higher } \kappa_K \text{ means denser, more compact clusters}).$$

Bounding box and fill ratio (lattice only). On the lattice we consider the minimal bounding box of K aligned with the lattice axes, with width w_K , height h_K and area $A_K = w_K h_K$. The fill ratio is

$$\phi_K = \frac{n_K}{A_K},$$

and we use $\min(w_K, h_K)$ and the elongation $\max(w_K, h_K)/\min(w_K, h_K)$ to detect thin or highly elongated clusters.

Interior holes (lattice only). Within the bounding box of K we consider the complement of K and count the finite connected components of this complement. The resulting number of interior holes is denoted H_K .

Diameter and aspect ratio (random-regular graph only). For components in random-regular networks, we approximate the graph-theoretic diameter

$$\delta_K = \max_{u, v \in K} \text{dist}_{G_C}(u, v),$$

and define an aspect ratio

$$\alpha_K = \frac{\delta_K}{\max(n_K - 1, 1)} \quad (\text{chain-like if } \alpha_K \text{ is large}).$$

We then classify each cluster K according to its descriptors. In particular:

$$\text{type}(K) = \begin{cases} \text{single_node}, & n_K = 1, \\ \text{star}_k + L, & K \text{ is a tree with no degree-2 nodes and } k \text{ high-degree centres with } L \text{ leaves,} \\ \text{large_cluster}, & n_K \geq 100, \end{cases}$$

and otherwise we proceed by topology.

On the 2D lattice we use the bounding box, fill ratio, holes and compactness:

$$\text{type}(K) = \begin{cases} \text{rectangle_}w_K \times h_K, & \phi_K = 1 \text{ and every site in the bounding box belongs to } K, \\ \text{chain_}n_K, & \min(w_K, h_K) = 1 \text{ or } \left(\frac{\max(w_K, h_K)}{\min(w_K, h_K)} \geq 3 \text{ and } \phi_K \geq 0.6\right), \\ \text{loop_}n_K, & H_K \geq 1, \\ \text{compact_}n_K, & \kappa_K > 1.5, \\ \text{irregular_}n_K, & \text{otherwise.} \end{cases}$$

On random-regular networks there is no geometric embedding, so we rely on edge count and diameter:

$$\text{type}(K) = \begin{cases} \text{cycle_}n_K, & e_K \geq n_K, \\ \text{chain_}n_K, & e_K < n_K \text{ and } \alpha_K > 0.7, \\ \text{irregular_}n_K, & \text{otherwise.} \end{cases}$$

In practice this classification is implemented exactly as in `classify_cluster_shape()` of our code, yielding human-readable labels such as "rectangle_4x5", "star_2+6", "compact_12" or "chain_5". These labels feed into our statistical analysis of cooperator-cluster morphologies over time.

2.3.4. Temporal stability of clusters. To distinguish persistent patterns from transient fluctuations, we compute the overlap between clusters at times $t - 1$ and t . A cluster at time t is labeled *stable* if its node set matches a cluster at time $t - 1$; otherwise, it is labeled *unstable*. We record the number of stable N_s and unstable N_u clusters at each step, and aggregate their type distributions to study persistence and volatility in cooperative organisation.

2.3.5. Data aggregation and visualisation. For each network type and temptation value T , we summarise the simulation output at the final time step $t = t_{\max} = 100$ by aggregating over the 1000 independent repetitions.

First, we compute the mean and standard deviation (across repetitions) of:

- the global cooperation level $f_C(t_{\max})$;
- the fractions of each strategy type at t_{\max} (consistent- C , consistent- D , oscillators);
- the numbers of stable and unstable cooperator clusters at t_{\max} .

These quantities are plotted as functions of T , with separate curves for each network type and shaded bands representing ± 1 standard deviation across repetitions. This yields summary profiles of cooperation, strategy composition, and cluster counts for each topology.

Second, for each network type, temptation value T and cluster shape label (motif) m , we compute the share of cooperator clusters of type m at the final time:

$$\text{share}(m \mid T) = \frac{N_m(T)}{N_{\text{tot}}(T)},$$

where both numerator and denominator are summed over all repetitions. We do this separately for stable and unstable clusters. The resulting motif compositions are shown as heatmaps with motif types on the vertical axis, T on the horizontal axis, and colour indicating $\text{share}(m \mid T, \text{network})$, allowing us to compare how the distribution of cluster morphologies changes across temptation regimes and between topologies.

3. RESULTS

3.1. General comparison of cooperation profiles and clusters: 2D lattice vs. Random-Regular graph. Figure 1 shows that the global cooperation curves $f_C(T)$ differ qualitatively across the two topologies even though size, degree and update rule are held fixed. On the 100×100 Moore lattice, cooperation remains high for most of $T \in [1, 1.55]$ and then collapses sharply as T approaches the geometric threshold $T_g = 5/3$, dropping from $f_C \approx 0.43$ at $T = 1.60$ to $f_C \approx 0.21$ at $T = 1.65$ and to $f_C \approx 2 \times 10^{-4}$ at $T \approx 1.67$ (Table 1). By contrast, on degree-8 random-regular graphs the decay begins much earlier: f_C is close to 0.92 only up to $T \approx 1.10$, then decreases steadily for $1.10 < T < 1.50$ (e.g., down to $f_C \approx 0.19$ at $T = 1.45$) and enters a rare-event plateau with $f_C = O(10^{-3})$ for $1.55 \leq T \leq 1.95$ (Table 2). The accompanying consistency metrics in Fig. 1 show the same contrast. The RR graph quickly becomes dominated by consistent defectors as T increases, whereas the lattice maintains a substantial cooperation until very near T_g .

Figure 2 and Tables 1–2 reveal that these macroscopic curves are reached through very different mesoscopic cluster organisation. On the lattice, low and moderate temptation typically lead to a macroscopic cooperative component (hence small $\langle N_u \rangle$ and, in the easiest cases, a stable component count near one), whereas the approach to T_g is marked by a surge of unstable clusters. For $T \approx 1.60$ – 1.66 we observe $\langle N_u \rangle \approx 60$ – 65 with essentially no stable clusters, consistent with a nucleation-limited slowdown rather than an immediate loss of brick viability. On the random-regular graph the intermediate regime $1.10 < T < 1.50$ is instead a fragmentation regime, where $\langle N_s \rangle$ collapses to zero and $\langle N_u \rangle$ grows by roughly two orders of magnitude, peaking around $\langle N_u \rangle \approx 180$ at $T = 1.45$ (Table 2). Only beyond $T \gtrsim 1.5$ does $\langle N_u \rangle$ fall back toward zero as the system settles into a small number of stable residual components ($\langle N_s \rangle \approx 2$ – 3 for much of $1.6 \leq T \leq 1.9$).

The motif census in Fig. 3 (see also the shares of dominant stable shapes in Tables 1 and 2) links these aggregate profiles to a small set of surviving motifs, which differs between the two networks. At high T on the lattice, stable cooperation is carried exclusively by fully cooperative rectangular bricks (3×3 or larger). On the random-regular graph, stable motifs at high T are instead almost entirely completed stars, primarily `star_1+8` and `star_2+14`. Thus, even at fixed degree $k = 8$, removing geometric embedding shifts the dominant resilient cooperative building blocks from compact rectangles to star-like traps. In both topologies, however, at extreme temptation the most frequent stable finite cooperator motif contains a cooperator vertex with $n = k$ cooperative neighbours.

3.2. Two-dimensional square lattice ($k = 8$).

3.2.1. Local payoff landscape of a 3×3 brick. Building on the local payoff analysis of rectangular domains in Szabó and Fáth [8], we re-derive the payoffs for a solitary 3×3 cooperative brick.

Let a solitary 3×3 block of cooperators be embedded in defectors. Using Moore neighbourhood ($k = 8$) with Prisoner’s Dilemma pay-offs $(R, S, T, P) = (1, 0, T, 0)$, the pay-off of every site in the 7×7 window centred on the brick is

$$\begin{array}{ccccccc}
 0 & 0 & 0 & 0 & 0 & 0 & 0 \\
 0 & T & 2T & 3T & 2T & T & 0 \\
 0 & 2T & 3 & 5 & 3 & 2T & 0 \\
 0 & 3T & 5 & 8 & 5 & 3T & 0 \\
 0 & 2T & 3 & 5 & 3 & 2T & 0 \\
 0 & T & 2T & 3T & 2T & T & 0 \\
 0 & 0 & 0 & 0 & 0 & 0 & 0
 \end{array} \tag{1}$$

We label this array as (1). Reading the four distinctive entries of (1) we find

Interior, side-border, and corner cooperators therefore earn, respectively,

$$\pi_C^{\text{int}} = 8, \quad \pi_C^{\text{side}} = 5, \quad \pi_C^{\text{corner}} = 3,$$

while the most fortunate defector surrounding the brick gets

$$\pi_D^{\text{max}} = 3T.$$

3.2.2. *Growth, marginal stability and decay.* Under unconditional imitation a node copies a neighbour only when that neighbour's pay-off is strictly larger. Inspection of the inequalities implied by (1) yields three dynamical regimes:

Condition on T	Dominant inequality	Regime
$T < 5/3$	$\pi_C^{\text{side}} > \pi_D^{\text{max}}$	growth
$5/3 \leq T < 8/3$	$\pi_D^{\text{max}} < \pi_C^{\text{int}}$ and $\pi_D^{\text{max}} \geq \pi_C^{\text{side}}$	stability
$T \geq 8/3$	$\pi_D^{\text{max}} > \pi_C^{\text{int}}$	decay

Because the numerical simulations are restricted to $T \leq 2$, only the first two regimes are observed in the data.

3.2.3. *Numerical census and kinetic interpretation.* Table 1 presents summary statistics for the lattice, including the fraction of cooperation, the numbers of stable and unstable cooperator clusters, and the share of stable clusters.

We define the rim-growth velocity as $v(T) \equiv 5 - 3T$, which quantifies the effective rate at which the boundary of a cooperative cluster advances in the lattice. This expression is derived under the simplifying assumption that the growing shape is an isolated 3×3 cooperator brick in a sea of defectors. While this velocity estimate is exact for such minimal brick shapes at the invasion threshold, it serves as an approximation in practice, since sub-critical shapes may exhibit slower growth.

- (a) $T < 1.60$. Most cooperators have coalesced into `large_clusters`, giving $\bar{f}_C \sim 0.945$. Even though $T = 1.0 < T_g = 5/3$ implies positive rim-growth velocity $v(T) = 5 - 3T = 2$, which should allow cooperative clusters to expand, cooperation fails to reach 100% due to the formation of defecting strips that never disappear. These “defector filaments” are 1D chains of defectors that can remain stable (see Fig. 4). As T increases to values like $T = 1.4$, these filaments thicken and percolate through the system, creating rugged frontiers between cooperator blocks (see Fig. 5). These patterns prevent cooperator clusters from merging, so the cooperation level stays below one even when the rim growth velocity is positive.
- (b) $1.60 < T < 1.67$. The velocity shrinks to 0.2. Consequently each snapshot is still populated by dozens of growing but unfinished domains ($\langle N_u \rangle \approx 65$ at $T = 1.66$), and $\bar{f}_C \sim 0.21$. The reduction is not due to a loss of growth capacity of the 3×3 or 3×4 rectangles (both still satisfy $3T < 5$). Rather, for $T \gtrsim 1.60$ all competing cooperator shapes—large, compact, irregular, or chain-like—either become unstable or stop expanding. These sub-critical shapes (i.e., compact and irregular motifs) are the dominant nucleation sites at $T < 1.60$, and once their growth halts the effective seed density falls by roughly two orders of magnitude, preventing percolation within $t = 99$. See Fig. 6.
- (c) $T = 5/3 \approx 1.67$. Now $v = 0$. Growth stops abruptly. Any cluster that is not a fully-saturated 3×3 (or larger rectangular) brick is erased in the very next timestep. Only those runs that had nucleated at least one brick before $t = 98$ retain cooperation, yielding $\bar{f}_C \approx 2.2 \times 10^{-4}$.
- (d) $1.67 < T \leq 2.0$. Bricks 3×3 (or any larger compact rectangle) are neutrally stable (i.e. neither growing nor shrinking) until $T > 8/3$ provided the first layer of surrounding defectors in its immediate rim are not boosted by stray cooperators (which is likely to happen in the first timesteps). As T increases towards 2, the payoff advantage of a boosted defector increases, which can explain the slight decline of $\bar{f}_C(T)$ reported in Table 1. See Fig. 7.

3.3. Random-regular network ($k = 8$).

3.3.1. *Local payoff landscape of a $(1+m)$ -star.* Because the RR topology contains no geometric blocks, the smallest self-sustaining cooperative structure is a star. Let a hub h (degree 8) be a cooperator and let m of its leaves ($0 \leq m \leq 8$) also be cooperators. A leaf d that is still a defector has

$$\pi_h = m, \quad \pi_d = \begin{cases} T & \text{if no other cooperative neighbour,} \\ qT & \text{if } q \geq 1 \text{ stray cooperators are adjacent to } d. \end{cases}$$

Under unconditional imitation $d \rightarrow C$ iff $\pi_h > \pi_d$. Hence

$$m > qT. \quad (2)$$

Equation (2) controls both star completion and erosion. Two limiting cases are important:

- **Isolated star ($q = 1$)**. A hub with $m \geq 3$ converts every missing spoke as long as $T < m$. In particular, an eight-leaf star (size 9) is always stable for $T < 8$.
- **Single stray cooperator ($q = 2$)**. If any stray C sits next to d the condition tightens to $m > 2T$. For $T \geq 1.6$ even a hub with $m = 5$ cannot beat a boosted defector. Incomplete stars freeze and later disappear.

3.3.2. Growth and arrest of star-like motifs.

Inequality (2) partitions the parameter space:

Condition on T	Star dynamics	Dominant clusters
$T < 1.10$	any $(1+m)$ -star with $m \geq 3$ self-completes	large merged domains
$1.10 \leq T < 1.50$	stars with $m \leq 5$ stall if $q = 2$	many unstable domains
$1.50 \leq T \leq 2.00$	isolated star-like motifs survive	star-like motifs

The transition around $T \approx 1.5$ is therefore *kinetic*, arising from the progressive failure of incomplete stars to finish recruiting their leaves.

Figures 12 and 13 display the `star_1+8` and `star_2+14` tree-like motifs, respectively, for visual reference.

3.3.3. Numerical census and kinetic interpretation. Table 2 summarises the behaviour of the degree-8 random-regular network at $t = 99$, reporting the global cooperation level f_C , the mean numbers of stable and unstable cooperator clusters $\langle N_s \rangle$ and $\langle N_u \rangle$, and the dominant stable motifs as a function of T . Figures 10 and 11 complement this census by displaying the full motif composition of stable and unstable clusters at $t = 99$ across temptation values. Together with the local star inequality (2) in Section 3.3.1, these statistics support a kinetic picture in which cooperation is limited by the completion of a small number of star-like traps, rather than by a collective phase transition.

- $T \leq 1.10$. For $T \in \{1.00, 1.05, 1.10\}$ the network almost always reaches a single macroscopic cooperative domain, with $f_C \approx 0.91\text{--}0.92$, $\langle N_s \rangle \approx 0.73$, and $\langle N_u \rangle \approx 0.26$ (Table 2). The motif census shows that essentially all stable clusters are labelled `large_cluster`, with share 1.000 at these values of T . This regime corresponds to the completion regime described in Section 3.3.2, where any $(1+m)$ -star with $m \geq 3$ quickly recruits its missing leaves and separate cooperative motifs tend to merge into larger components. See Fig. 14.
- $1.10 < T < 1.50$. As T increases beyond 1.10, f_C decays monotonically from 0.635 at $T = 1.15$ to 0.190 at $T = 1.45$, while $\langle N_s \rangle$ collapses to zero and $\langle N_u \rangle$ grows by two orders of magnitude, reaching $\langle N_u \rangle \approx 180$ at $T = 1.45$ (Table 2). Figure 11 shows that these unstable components are dominated by isolated cooperators (`single_node`), with a smaller contribution from remnants of `large_cluster` components and short `chain_2/chain_3` fragments. This is consistent with a fragmentation regime in which many cooperative seeds appear but fail to consolidate into persistent traps by $t = 99$. Kinetically, this is the regime where boosted defectors begin to obstruct star completion. When a missing spoke has additional cooperative neighbours, its payoff increases to qT and the completion condition $m > qT$ becomes harder to satisfy. In particular, for $q = 2$ the requirement becomes $m > 2T$, so as T approaches 1.5 incomplete stars with small m (e.g., $m \leq 3$) cannot finish recruiting their leaves, and larger q makes completion even less likely. Because the random-regular graph is locally tree-like, perturbations from stray cooperators occur across many leaves, so partial stars are increasingly blocked rather than completed. The result is many unstable fragments and a drop in global cooperation. See Fig. 15.
- $T \geq 1.50$. Beyond $T \approx 1.5$ the system enters a rare-event plateau. The average cooperation level drops from $f_C \approx 7 \times 10^{-2}$ at $T = 1.50$ to $f_C \sim 10^{-3}$ for $1.55 \leq T \leq 1.95$, and down to $f_C \approx 2.6 \times 10^{-4}$ at $T = 2.00$ (Table 2). At the same time $\langle N_u \rangle$ falls back to essentially zero, while the number of stable clusters stabilises around $\langle N_s \rangle \approx 2\text{--}3$ for $1.60 \leq T \leq 1.80$. The motif census in Table 2 and the stable-cluster heatmap (Fig. 10) show that these surviving components are almost exclusively `star_1+8` and `star_2+14` trees, with combined shares above 0.80 for all $T \gtrsim 1.6$. Other motifs (cycles, chains,

irregular clusters) are either transient or statistically negligible at $t = 99$, and only a small number of tiny `chain_3` motifs appear as stable at $T = 2.0$. See Fig. 16.

In summary, at high values of T , residual cooperation is explained by the early appearance of a few fully completed stars. Completed stars are extremely rare under random initial conditions because they require a perfectly coordinated local neighbourhood and must avoid interference from nearby stray cooperators during the first time steps. Crucially, once a star is complete, inequality (2) implies neutral stability for all $T < 8$, so in our range $T \leq 2$ the stability of completed stars is essentially T -independent. The observed decay of $f_C(T)$ in Table 2 is therefore not driven by an intrinsic loss of stability of completed stars, but by a kinetic bottleneck. As T increases, incomplete stars and other cooperative fragments are progressively blocked by boosted defectors, fail to complete, and are eventually eroded.

4. CONCLUSION

In this paper we revisited the spatial Prisoner’s Dilemma using exactly the parameter set of the canonical Nowak and May study, so that our results can be read as a direct extension of their seminal work [7].

Across $R = 1000$ runs on networks of size $N = 10^4$ (with $t_{\max} = 99$), using degree $k = 8$, payoffs $(R, S, T, P) = (1, 0, T, 0)$ with $T \in [1, 2]$, and synchronous unconditional imitation, we find two robust signatures at high T . First, on the two-dimensional Moore lattice, for $T > 5/3$ every connected cooperator component that persists in an absorbing configuration is a fully occupied rectangle whose side lengths are at least 3 (i.e., a $w \times h$ brick with $w, h \geq 3$). Second, on random-regular graphs, for $T \gtrsim 1.5$ stable cooperator components are dominated by fully completed stars (primarily `star_1+8` and `star_2+14`), while other shapes are rare.

In both topologies studied here, the most frequent surviving motif at high T contains a cooperator whose entire neighbourhood is cooperative ($n = k = 8$). This suggests a broader hypothesis: at high T , under payoffs $(R, S, T, P) = (1, 0, T, 0)$ and synchronous unconditional imitation on k -regular graphs, once the dynamics becomes nucleation limited, the most frequent stable finite cooperator component is a motif that contains a cooperator vertex with $n = k$ cooperative neighbours (equivalently, a cooperator whose entire neighbourhood is cooperative).

Furthermore, in both topologies the cooperation drop is mainly kinetic. It is not driven by a sudden loss of intrinsic viability of the most resilient motifs (bricks on the lattice, completed stars on RR graphs), which remain stable in the relevant parameter range. Instead, as T increases the dynamics becomes increasingly dominated by interference. That is, subcritical shapes stop expanding, and stray cooperators boost nearby defectors, creating local noise that blocks the completion of growing motifs. The effective density of successful seeds then collapses, so cooperative domains fail to coalesce and the global cooperation level drops.

Our results reinforce a central lesson from three decades of work on spatial evolutionary games [8, 9, 13, 14, 15], namely, network reciprocity is not one mechanism but a family of mechanisms whose effectiveness depends on the update rule, the topology, and the relevant time-scales. From an engineering viewpoint, a key implication is that cooperation at high temptation is limited not only by payoffs but also by structural and physical constraints that determine which local cooperative patterns can actually assemble and persist. This resonates with recent work showing that physicality can strongly shape network structure and function [16, 17, 18, 19]. More broadly, it remains an active research question how small initial shocks, homophily, and local cluster concentration shape complex contagion and collective outcomes [20, 21, 22, 23]. Two avenues for future research remain open: first, to derive analytical results that confirm our numerical findings; and second, to test how far they generalise to networks with different degrees.

DATA AVAILABILITY

Electronic supplementary material and simulation code are available at https://github.com/jsegoviamartin/Topological_traps_in_evolutionary_games and [24].

REFERENCES

[1] W. D. Hamilton. The genetical evolution of social behaviour. i & ii. *Journal of Theoretical Biology*, 7: 1–52, 1964. doi: 10.1016/0022-5193(64)90038-4.

- [2] Garrett Hardin. The tragedy of the commons. *Science*, 162:1243–1248, 1968. doi: 10.1126/science.162.3859.1243.
- [3] Elizabeth Pennisi. How did cooperative behavior evolve? *Science*, 309(5731):93, 2005. doi: 10.1126/science.309.5731.93.
- [4] Robert Axelrod. *The Evolution of Cooperation*. Basic Books, New York, 1984.
- [5] John Maynard Smith. *Evolution and the Theory of Games*. Cambridge University Press, Cambridge, 1982.
- [6] Martin A. Nowak. Five rules for the evolution of cooperation. *Science*, 314:1560–1563, 2006. doi: 10.1126/science.1133755.
- [7] Martin A. Nowak and Robert M. May. Evolutionary games and spatial chaos. *Nature*, 359:826–829, 1992. doi: 10.1038/359826a0.
- [8] Gábor Szabó and Géza Fáth. Evolutionary games on graphs. *Physics Reports*, 446:97–216, 2007. doi: 10.1016/j.physrep.2007.04.004.
- [9] Carlos P. Roca, José A. Cuesta, and Angel Sánchez. Evolutionary game theory: Temporal and spatial effects beyond replicator dynamics. *Physics of Life Reviews*, 6:208–249, 2009. doi: 10.1016/j.plrev.2009.08.001.
- [10] Peter D. Taylor and Leo B. Jonker. Evolutionarily stable strategies and game dynamics. *Mathematical Biosciences*, 40:145–156, 1978. doi: 10.1016/0025-5564(78)90077-9.
- [11] Josef Hofbauer and Karl Sigmund. *Evolutionary Games and Population Dynamics*. Cambridge University Press, Cambridge, 1998.
- [12] John Nash. Equilibrium points in n -person games. *Proceedings of the National Academy of Sciences of the United States of America*, 36:48–49, 1950. doi: 10.1073/pnas.36.1.48.
- [13] Hisashi Ohtsuki, Christoph Hauert, Erez Lieberman, and Martin A. Nowak. A simple rule for the evolution of cooperation on graphs and social networks. *Nature*, 441:502–505, 2006. doi: 10.1038/nature04605.
- [14] Arne Traulsen, Jens Christian Claussen, and Christoph Hauert. Coevolutionary dynamics: From finite to infinite populations. *Physical Review Letters*, 95:238701, 2006. doi: 10.1103/PhysRevLett.95.238701.
- [15] José A. Cuesta, Ricardo Jiménez, and Angel Sánchez. Reward and cooperation in spatial games. In Gábor Szabó et al., editor, *Games, Epidemics, and Sociophysics*, pages 27–46. Springer, Berlin, 2015. doi: 10.1007/978-3-319-13362-5_3.
- [16] Márton Pósfai, Balázs Szegedy, Iva Bačić, Luka Blagojević, Miklós Abért, János Kertész, László Lovász, and Albert-László Barabási. Impact of physicality on network structure. *Nature Physics*, 20(1):142–149, 2024.
- [17] Arkadiusz Stopczynski, Alex ‘Sandy’ Pentland, and Sune Lehmann. How physical proximity shapes complex social networks. *Scientific reports*, 8(1):17722, 2018.
- [18] Niek Kerssies, Jose Segovia Martin, and James Winters. Connect-while-in-range: modelling the impact of spatial constraints on dynamic communication network structures. *arXiv preprint arXiv:2410.13527*, 2024.
- [19] José Segovia-Martín, Bradley Walker, Nicolas Fay, and Monica Tamariz. Network connectivity dynamics, cognitive biases, and the evolution of cultural diversity in round-robin interactive micro-societies. *Cognitive Science*, 44(7):e12852, 2020.
- [20] Miller McPherson, Lynn Smith-Lovin, and James M Cook. Birds of a feather: Homophily in social networks. *Annual review of sociology*, 27(1):415–444, 2001.
- [21] Duncan J Watts. A simple model of global cascades on random networks. *Proceedings of the National Academy of Sciences*, 99(9):5766–5771, 2002.
- [22] Damon Centola. The spread of behavior in an online social network experiment. *science*, 329(5996):1194–1197, 2010.
- [23] Jose Segovia-Martin and Óscar Rivero. Cross-border political competition. *Plos one*, 19(5):e0297731, 2024.
- [24] Jose Segovia Martin. Topological motifs in evolutionary games: comparing cooperation on 2-d lattices and random-regular graphs. 2025. URL <https://hdl.handle.net/10609/153400>.

¹ SCHOOL OF COLLECTIVE INTELLIGENCE (M6 POLYTECHNIC UNIVERSITY)

² COMPLEX SYSTEMS INSTITUTE OF PARIS ILE-DE-FRANCE (ISCPiF-CNRS)

Email address: Jose.Segovia@um6p.ma

LIST OF FIGURES

1 Final-step ($t = 99$) network-level metrics as a function of temptation T for 2D lattices and random-regular graphs. Lines show means across repetitions; shaded regions indicate ± 1 standard deviation. 12

2 Mean number of stable (N_s) and unstable (N_u) cooperator clusters at $t = 99$ as a function of temptation T , for 2D lattices and random-regular graphs. Shaded regions indicate ± 1 standard deviation. 13

3 Share of stable and unstable clusters by motif type and temptation at $t = 99$ for 2D lattices and Random-Regular graphs. 14

4 Time evolution of cooperator clusters on a 100×100 lattice for $T = 1.0$. Snapshots at time steps $t = 0, 1, 2, 3, 4, 99$ show the expansion of cooperative motifs and the persistence of defecting filaments. 15

5 Time evolution of cooperator clusters on a 100×100 lattice for $T = 1.4$. Snapshots at time steps $t = 0, 1, 2, 3, 4, 99$ illustrate the expansion of cooperative bricks and other irregular shapes and the stability of certain defector structures at $t = 99$. 16

6 Time evolution of cooperator clusters on a 100×100 lattice for $T = 1.6$. Snapshots at time steps $t = 0, 1, 2, 3, 4, 99$ show the limited expansion of sub-critical cooperative shapes and the persistence of defecting shapes at $t = 99$. 17

7 Time evolution of cooperator clusters on a 100×100 lattice for $T = 1.7$. Snapshots at time steps $t = 0, 1, 2, 3, 4, 99$ show an abrupt halt to all growth. Only 3x3 (or larger bricks) are stable. 18

8 Stable cooperator cluster motif composition at $t = 99$ for 2D lattices. Each cell shows the share of clusters of a given motif at temptation T ; light grey cells correspond to zero frequency. 19

9 Unstable cooperator cluster motif composition at $t = 99$ for 2D lattices. 20

10 Stable cooperator cluster motif composition at $t = 99$ for random-regular graphs. 21

11 Unstable cooperator cluster motif composition at $t = 99$ for random-regular graphs. 22

12 **star_1+8** star found on the degree-8 random-regular network for $T \gtrsim 1.5$. One hub (pay-off 8) feeds eight leaves; each leaf therefore sees a neighbour with pay-off $8 > T$ and never imitates an outside defector. The configuration is neutrally stable for every $T < 8$. 23

13 **star_2+14** star: two connected hubs (each pay-off 8) jointly serve fourteen leaves, yielding the same stability condition as the 1+8 star. Such twin-hub stars dominate the residual cooperation plateau for $T \gtrsim 1.5$ when they manage to nucleate in the initial timesteps. 24

14 Time evolution of cooperator clusters on a 100×100 random-regular graph for $T = 1.0$. Snapshots at time steps $t = 0, 1, 2, 3, 4, 99$ illustrate the expansion of cooperative bricks and other irregular shapes and the stability of certain defector structures at $t = 99$. 25

15 Time evolution of cooperator clusters on a 100×100 random-regular graph for $T = 1.4$. Snapshots at time steps $t = 0, 1, 2, 3, 4, 99$ illustrate the expansion of cooperative bricks and other irregular shapes and the stability of certain defector structures at $t = 99$. 26

16 Time evolution of cooperator clusters on a 100×100 random-regular graph for $T = 1.8$. Snapshots at time steps $t = 0, 1, 2, 3, 4, 99$ illustrate the expansion of cooperative bricks and other irregular shapes and the stability of certain defector structures at $t = 99$. 27

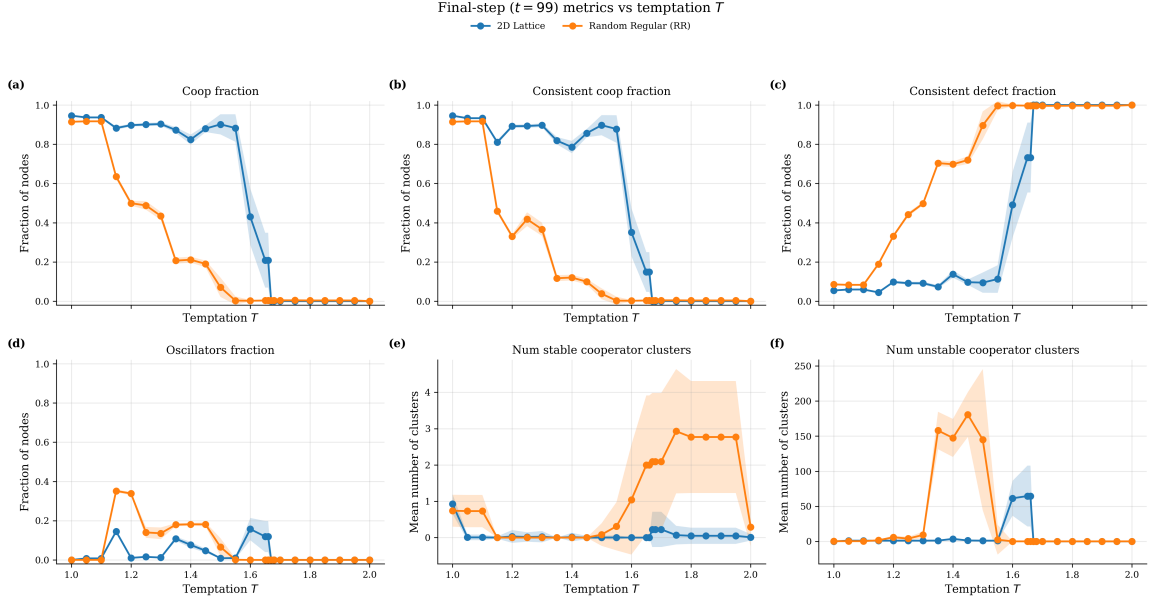


FIGURE 1. Final-step ($t = 99$) network-level metrics as a function of temptation T for 2D lattices and random-regular graphs. Lines show means across repetitions; shaded regions indicate ± 1 standard deviation.

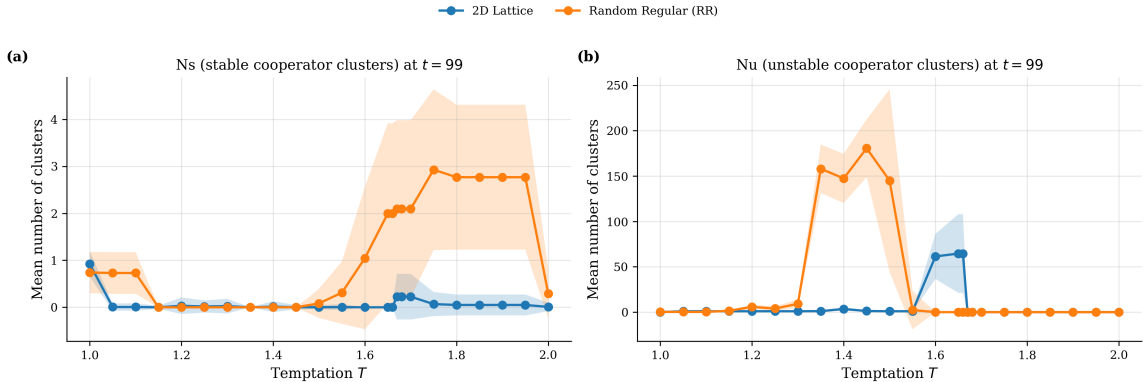


FIGURE 2. Mean number of stable (N_s) and unstable (N_u) cooperator clusters at $t = 99$ as a function of temptation T , for 2D lattices and random-regular graphs. Shaded regions indicate ± 1 standard deviation.

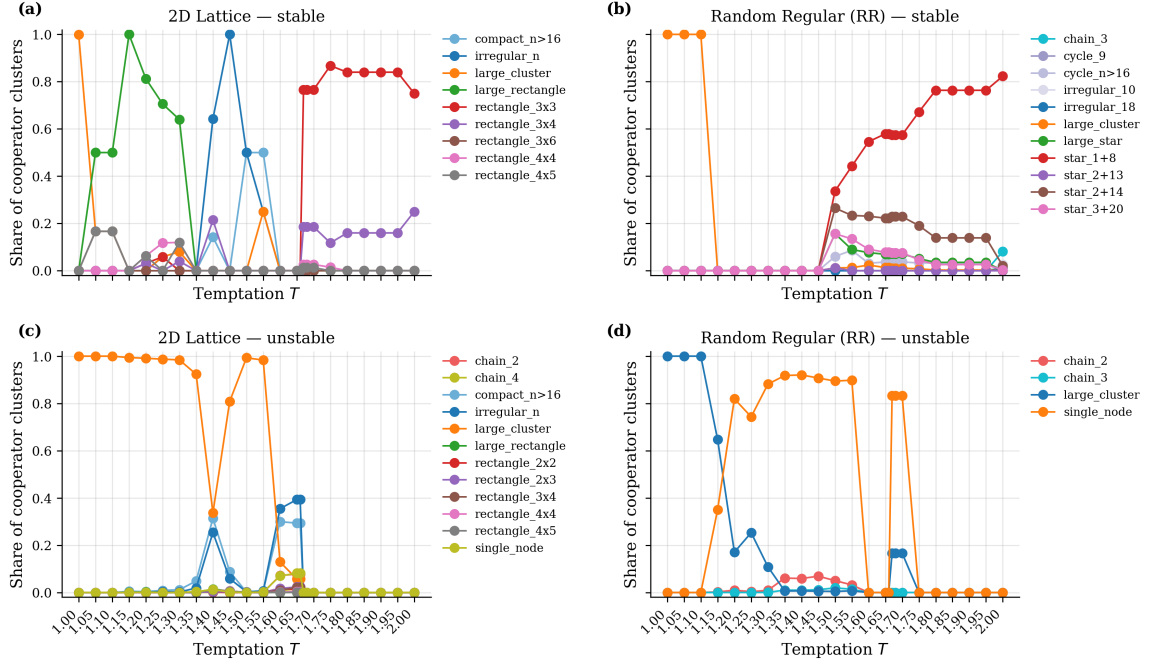
Share of cooperator clusters by motif and temptation ($t = 99$)

FIGURE 3. Share of stable and unstable clusters by motif type and temptation at $t = 99$ for 2D lattices and Random-Regular graphs.

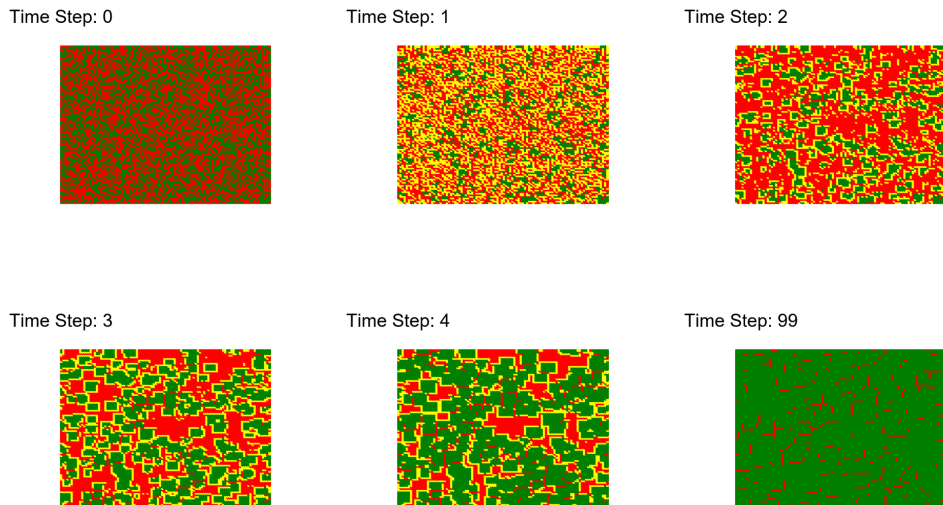


FIGURE 4. Time evolution of cooperator clusters on a 100×100 lattice for $T = 1.0$. Snapshots at time steps $t = 0, 1, 2, 3, 4, 99$ show the expansion of cooperative motifs and the persistence of defecting filaments.

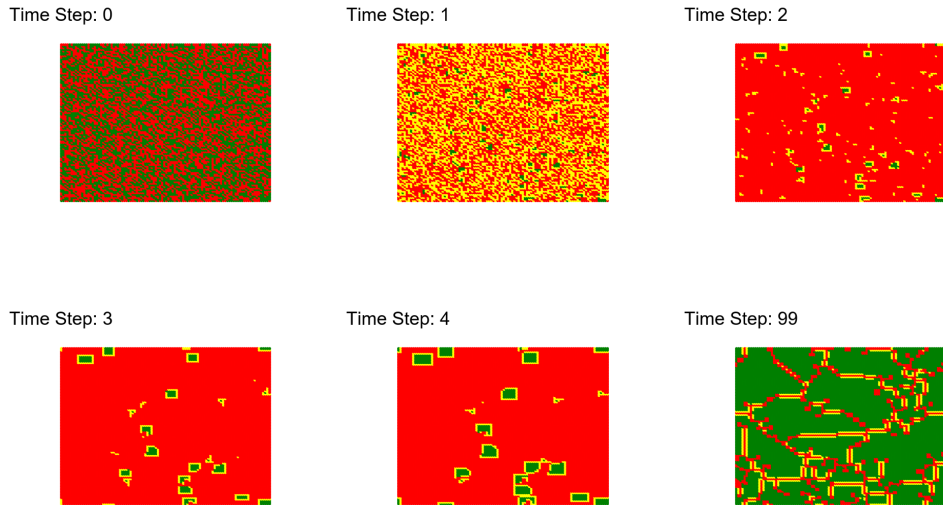


FIGURE 5. Time evolution of cooperator clusters on a 100×100 lattice for $T = 1.4$. Snapshots at time steps $t = 0, 1, 2, 3, 4, 99$ illustrate the expansion of cooperative bricks and other irregular shapes and the stability of certain defector structures at $t = 99$.

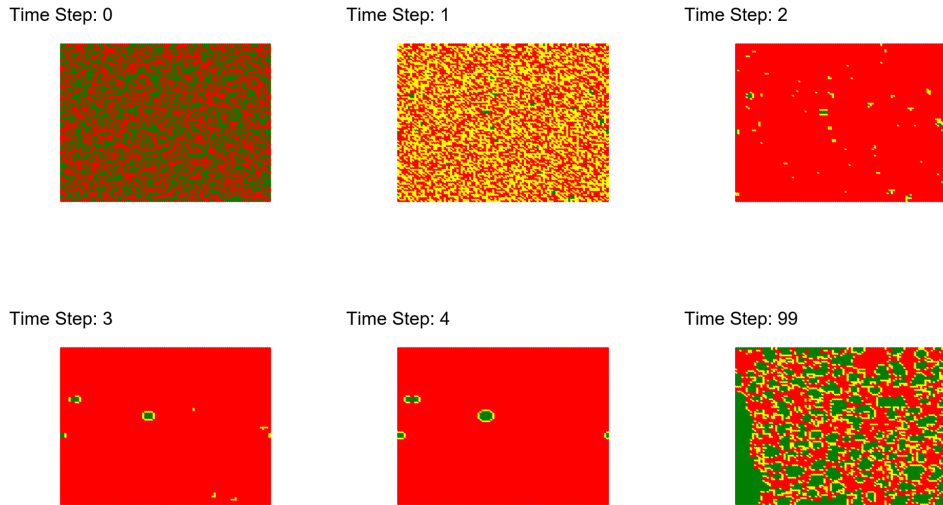


FIGURE 6. Time evolution of cooperator clusters on a 100×100 lattice for $T = 1.6$. Snapshots at time steps $t = 0, 1, 2, 3, 4, 99$ show the limited expansion of sub-critical cooperative shapes and the persistence of defecting shapes at $t = 99$.

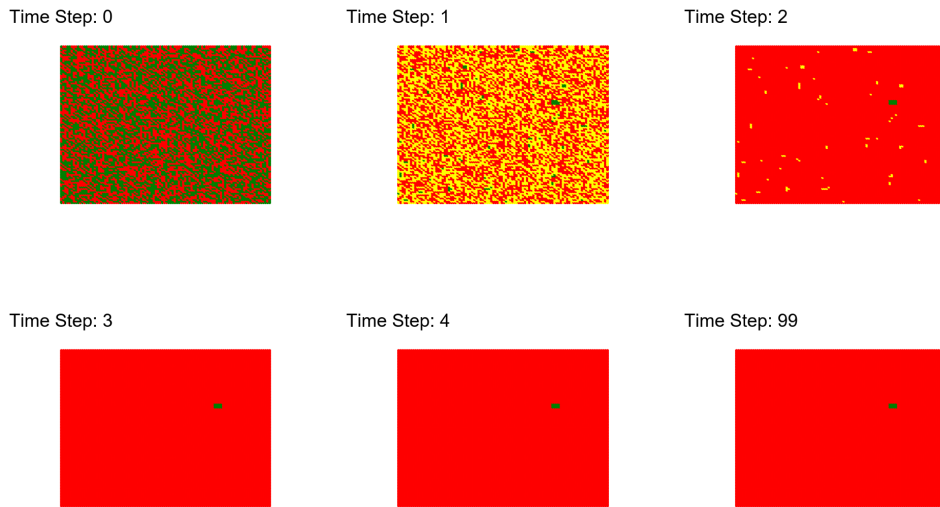


FIGURE 7. Time evolution of cooperator clusters on a 100×100 lattice for $T = 1.7$. Snapshots at time steps $t = 0, 1, 2, 3, 4, 99$ show an abrupt halt to all growth. Only 3x3 (or larger bricks) are stable.

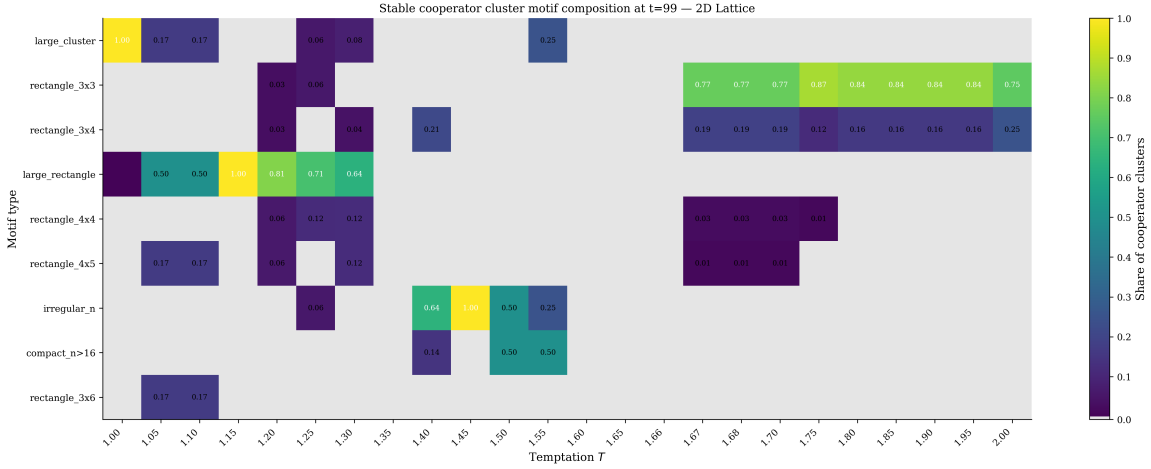


FIGURE 8. Stable cooperator cluster motif composition at $t = 99$ for 2D lattices. Each cell shows the share of clusters of a given motif at temptation T ; light grey cells correspond to zero frequency.

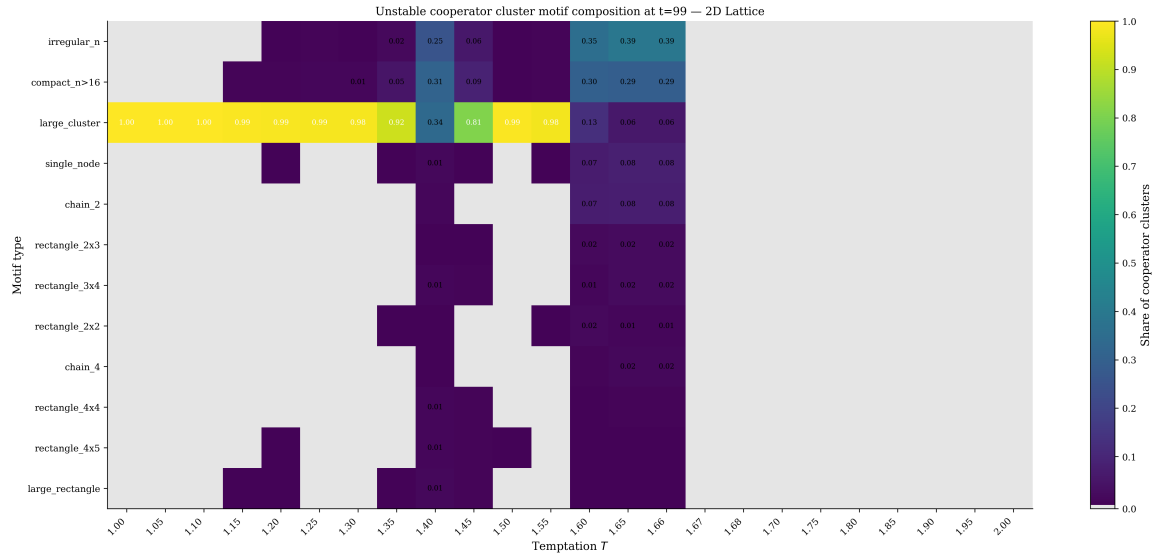


FIGURE 9. Unstable cooperator cluster motif composition at $t = 99$ for 2D lattices.

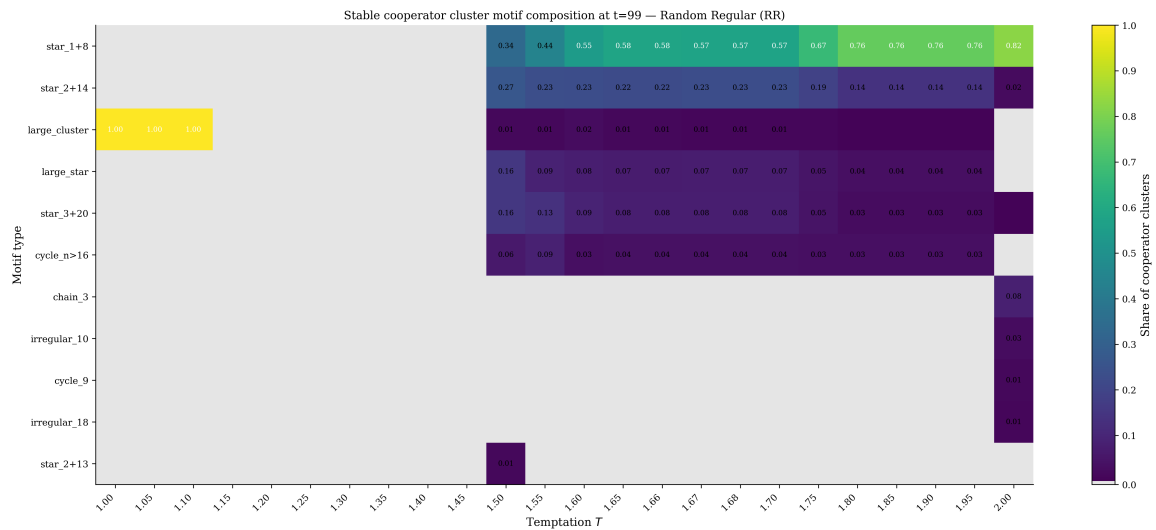


FIGURE 10. Stable cooperator cluster motif composition at $t = 99$ for random-regular graphs.

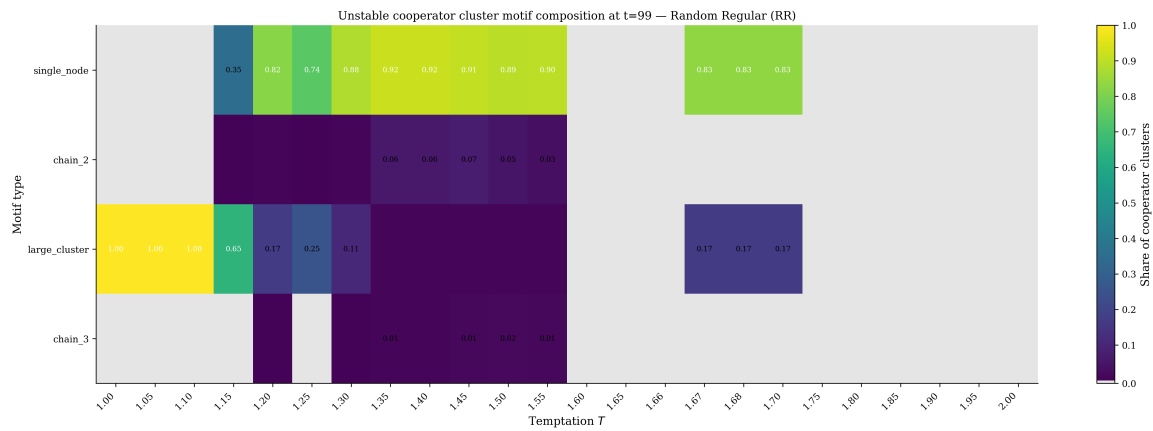


FIGURE 11. Unstable cooperator cluster motif composition at $t = 99$ for random-regular graphs.

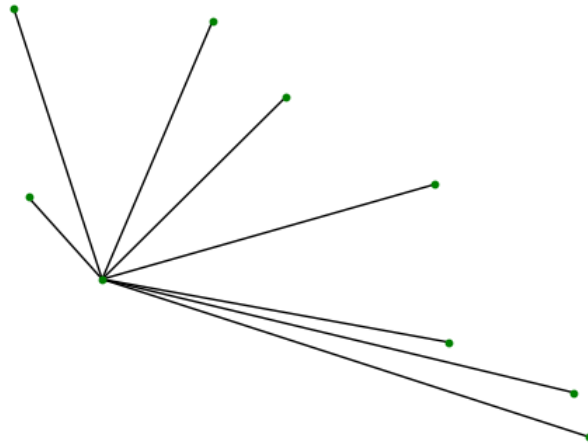


FIGURE 12. **star_1+8** star found on the degree-8 random-regular network for $T \gtrsim 1.5$. One hub (pay-off 8) feeds eight leaves; each leaf therefore sees a neighbour with pay-off $8 > T$ and never imitates an outside defector. The configuration is neutrally stable for every $T < 8$.

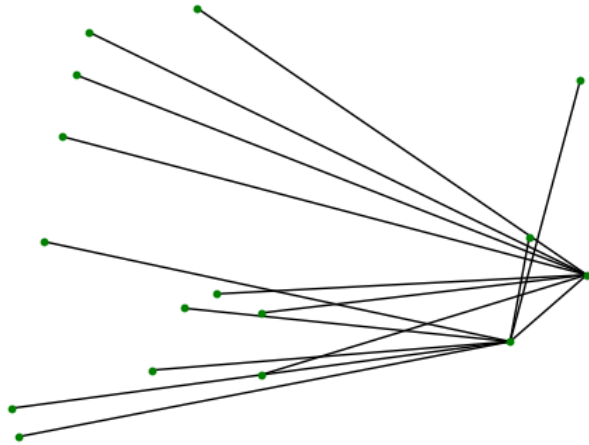


FIGURE 13. **star_2+14** star: two connected hubs (each pay-off 8) jointly serve fourteen leaves, yielding the same stability condition as the 1 + 8 star. Such twin-hub stars dominate the residual cooperation plateau for $T \gtrsim 1.5$ when they manage to nucleate in the initial timesteps.

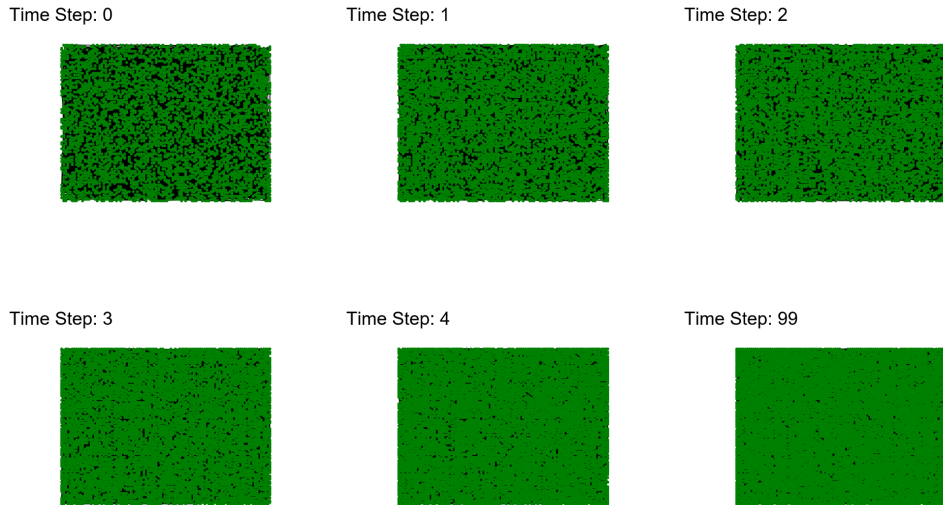


FIGURE 14. Time evolution of cooperator clusters on a 100×100 random-regular graph for $T = 1.0$. Snapshots at time steps $t = 0, 1, 2, 3, 4, 99$ illustrate the expansion of cooperative bricks and other irregular shapes and the stability of certain defector structures at $t = 99$.

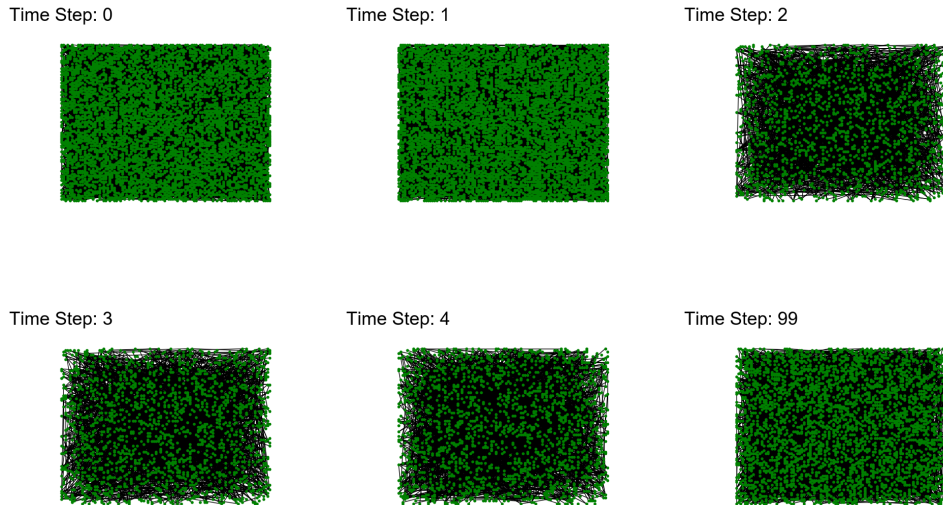


FIGURE 15. Time evolution of cooperator clusters on a 100×100 random-regular graph for $T = 1.4$. Snapshots at time steps $t = 0, 1, 2, 3, 4, 99$ illustrate the expansion of cooperative bricks and other irregular shapes and the stability of certain defector structures at $t = 99$.

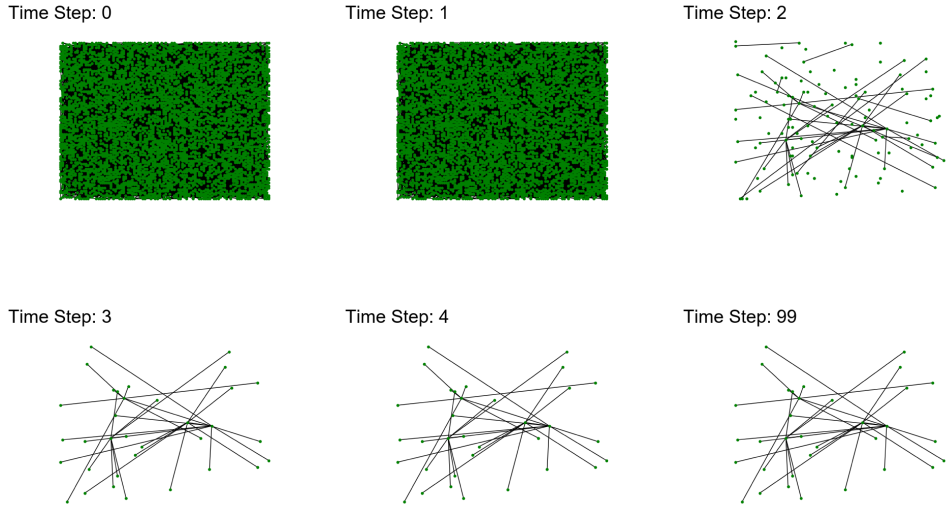


FIGURE 16. Time evolution of cooperator clusters on a 100×100 random-regular graph for $T = 1.8$. Snapshots at time steps $t = 0, 1, 2, 3, 4, 99$ illustrate the expansion of cooperative bricks and other irregular shapes and the stability of certain defector structures at $t = 99$.

LIST OF TABLES

1 Square-lattice cluster statistics at $t = 99$. Results are averaged over $R = 1000$ independent runs. One-sigma run-to-run fluctuations are reported for f_C . N_s stands for the mean number of stable cooperator clusters at $t = 99$. N_u stands for the mean number of unstable cooperator clusters at $t = 99$. The last column lists the two most frequent stable shapes and their relative shares of cooperator clusters. 29

2 Random-regular cluster statistics at $t = 99$. Results are averaged over $R = 1000$ independent runs. One-sigma run-to-run fluctuations are reported for f_C . N_s stands for the mean number of stable cooperator clusters at $t = 99$. N_u stands for the mean number of unstable cooperator clusters at $t = 99$. The last column lists the two most frequent stable shapes and their relative shares of cooperator clusters. 30

TABLE 1. Square-lattice cluster statistics at $t = 99$. Results are averaged over $R = 1000$ independent runs. One-sigma run-to-run fluctuations are reported for f_C . N_s stands for the mean number of stable cooperator clusters at $t = 99$. N_u stands for the mean number of unstable cooperator clusters at $t = 99$. The last column lists the two most frequent stable shapes and their relative shares of cooperator clusters.

T	$f_C \pm \sigma$	$\langle N_s \rangle \pm \sigma$	$\langle N_u \rangle \pm \sigma$	Dominant stable shapes (share)
1.00	0.945 ± 0.004	0.924 ± 0.269	0.077 ± 0.267	large_cluster (0.999), large_rectangle (0.001)
1.05	0.937 ± 0.004	0.006 ± 0.077	0.999 ± 0.032	large_rectangle (0.500), large_cluster (0.167)
1.10	0.937 ± 0.004	0.006 ± 0.077	0.999 ± 0.032	large_rectangle (0.500), large_cluster (0.167)
1.15	0.882 ± 0.009	0.001 ± 0.032	1.006 ± 0.077	large_rectangle (1.000)
1.20	0.897 ± 0.007	0.032 ± 0.176	1.012 ± 0.109	large_rectangle (0.812), rectangle_4x4 (0.062)
1.25	0.900 ± 0.008	0.017 ± 0.129	1.014 ± 0.118	large_rectangle (0.706), rectangle_4x4 (0.118)
1.30	0.903 ± 0.009	0.025 ± 0.156	1.018 ± 0.133	large_rectangle (0.640), rectangle_4x4 (0.120)
1.35	0.873 ± 0.014	0.000 ± 0.000	1.111 ± 0.356	—
1.40	0.824 ± 0.025	0.014 ± 0.118	3.501 ± 2.002	irregular_n (0.643), rectangle_3x4 (0.214)
1.45	0.880 ± 0.017	0.002 ± 0.045	1.248 ± 0.579	irregular_n (1.000)
1.50	0.901 ± 0.051	0.002 ± 0.045	1.004 ± 0.100	compact_n>16 (0.500), irregular_n (0.500)
1.55	0.883 ± 0.070	0.004 ± 0.063	1.013 ± 0.144	compact_n>16 (0.500), irregular_n (0.250)
1.60	0.430 ± 0.143	0.000 ± 0.000	61.404 ± 24.832	—
1.65	0.209 ± 0.140	0.000 ± 0.000	64.600 ± 43.345	—
1.66	0.209 ± 0.140	0.000 ± 0.000	64.600 ± 43.345	—
1.67	$2.2 \times 10^{-4} \pm 4.9 \times 10^{-4}$	0.226 ± 0.485	0.000 ± 0.000	rectangle_3x3 (0.765), rectangle_3x4 (0.186)
1.68	$2.2 \times 10^{-4} \pm 4.9 \times 10^{-4}$	0.226 ± 0.485	0.000 ± 0.000	rectangle_3x3 (0.765), rectangle_3x4 (0.186)
1.70	$2.2 \times 10^{-4} \pm 4.9 \times 10^{-4}$	0.226 ± 0.485	0.000 ± 0.000	rectangle_3x3 (0.765), rectangle_3x4 (0.186)
1.75	$6.4 \times 10^{-5} \pm 2.4 \times 10^{-4}$	0.068 ± 0.256	0.000 ± 0.000	rectangle_3x3 (0.868), rectangle_3x4 (0.118)
1.80	$4.7 \times 10^{-5} \pm 2.1 \times 10^{-4}$	0.050 ± 0.223	0.000 ± 0.000	rectangle_3x3 (0.840), rectangle_3x4 (0.160)
1.85	$4.7 \times 10^{-5} \pm 2.1 \times 10^{-4}$	0.050 ± 0.223	0.000 ± 0.000	rectangle_3x3 (0.840), rectangle_3x4 (0.160)
1.90	$4.7 \times 10^{-5} \pm 2.1 \times 10^{-4}$	0.050 ± 0.223	0.000 ± 0.000	rectangle_3x3 (0.840), rectangle_3x4 (0.160)
1.95	$4.7 \times 10^{-5} \pm 2.1 \times 10^{-4}$	0.050 ± 0.223	0.000 ± 0.000	rectangle_3x3 (0.840), rectangle_3x4 (0.160)
2.00	$7.8 \times 10^{-6} \pm 8.8 \times 10^{-5}$	0.008 ± 0.089	0.000 ± 0.000	rectangle_3x3 (0.750), rectangle_3x4 (0.250)

TABLE 2. Random-regular cluster statistics at $t = 99$. Results are averaged over $R = 1000$ independent runs. One-sigma run-to-run fluctuations are reported for f_C . N_s stands for the mean number of stable cooperator clusters at $t = 99$. N_u stands for the mean number of unstable cooperator clusters at $t = 99$. The last column lists the two most frequent stable shapes and their relative shares of cooperator clusters.

T	$f_C \pm \sigma$	$\langle N_s \rangle \pm \sigma$	$\langle N_u \rangle \pm \sigma$	Dominant stable shapes (share)
1.00	0.914 ± 0.003	0.740 ± 0.439	0.260 ± 0.439	large_cluster (1.000)
1.05	0.917 ± 0.003	0.730 ± 0.444	0.270 ± 0.444	large_cluster (1.000)
1.10	0.917 ± 0.003	0.730 ± 0.444	0.270 ± 0.444	large_cluster (1.000)
1.15	0.635 ± 0.011	0.000 ± 0.000	1.546 ± 0.727	—
1.20	0.499 ± 0.012	0.000 ± 0.000	5.858 ± 2.377	—
1.25	0.488 ± 0.022	0.000 ± 0.000	3.952 ± 2.402	—
1.30	0.434 ± 0.020	0.000 ± 0.000	9.199 ± 4.739	—
1.35	0.207 ± 0.015	0.000 ± 0.000	158.037 ± 26.669	—
1.40	0.211 ± 0.015	0.000 ± 0.000	147.425 ± 27.103	—
1.45	0.190 ± 0.017	0.000 ± 0.000	180.654 ± 31.886	—
1.50	0.071 ± 0.049	0.083 ± 0.310	145.008 ± 100.554	star_1+8 (0.337), star_2+14 (0.265)
1.55	0.003 ± 0.021	0.312 ± 0.664	2.377 ± 21.226	star_1+8 (0.442), star_2+14 (0.234)
1.60	0.002 ± 0.004	1.044 ± 1.511	0.000 ± 0.000	star_1+8 (0.546), star_2+14 (0.231)
1.65	0.003 ± 0.004	1.997 ± 1.916	0.000 ± 0.000	star_1+8 (0.579), star_2+14 (0.222)
1.66	0.003 ± 0.004	1.997 ± 1.916	0.000 ± 0.000	star_1+8 (0.579), star_2+14 (0.222)
1.67	0.004 ± 0.008	2.094 ± 1.887	0.006 ± 0.190	star_1+8 (0.575), star_2+14 (0.229)
1.68	0.004 ± 0.008	2.094 ± 1.887	0.006 ± 0.190	star_1+8 (0.575), star_2+14 (0.229)
1.70	0.004 ± 0.008	2.094 ± 1.887	0.006 ± 0.190	star_1+8 (0.575), star_2+14 (0.229)
1.75	0.004 ± 0.003	2.928 ± 1.710	0.000 ± 0.000	star_1+8 (0.672), star_2+14 (0.191)
1.80	0.004 ± 0.003	2.769 ± 1.541	0.000 ± 0.000	star_1+8 (0.763), star_2+14 (0.139)
1.85	0.004 ± 0.003	2.769 ± 1.541	0.000 ± 0.000	star_1+8 (0.763), star_2+14 (0.139)
1.90	0.004 ± 0.003	2.769 ± 1.541	0.000 ± 0.000	star_1+8 (0.763), star_2+14 (0.139)
1.95	0.004 ± 0.003	2.769 ± 1.541	0.000 ± 0.000	star_1+8 (0.763), star_2+14 (0.139)
2.00	$2.6 \times 10^{-4} \pm 5.0 \times 10^{-4}$	0.293 ± 0.530	0.000 ± 0.000	star_1+8 (0.823), chain_3 (0.082)